arXiv:1504.05836v1 [hep-ph] 22 Apr 2015

Probing Charged Higgs Boson Couplings at the FCC-hh Collider

I.T. Cakir,* S. Kuday,† and H. Saygin‡

Istanbul Aydin University, Application and Research Center for Advanced Studies, 34295 Sefakoy, Istanbul, Turkey

A. Senol§

Abant Izzet Baysal University, Department of Physics, 14280 Golkoy, Bolu, Turkey

O. Cakir¶

Istanbul Aydin University, Application and Research Center for Advanced Studies, 34295 Sefakoy, Istanbul, Turkey and

Ankara University, Department of Physics, 06100 Tandogan, Ankara, Turkey

(Dated: March 4, 2022)

Abstract

Many of the new physics models predicts a light Higgs boson similar to the Higgs boson of the Standard Model (SM) and also extra scalar bosons. Beyond the search channels for a SM Higgs boson, the future collider experiments will explore additional channels that are specific to extended Higgs sectors. We study the charged Higgs boson production within the framework of two Higgs doublet models (THDM) in the proton-proton collisions at the FCC-hh collider. With an integrated luminosity of 500 fb^{-1} at very high energy frontier, we obtain a significant coverage of the parameter space and distinguish the charged Higgs-top-bottom interaction within the THDM or other new physics models with charged Higgs boson mass up to 1 TeV.

* ilkayturkcakir@aydin.edu.tr

† sinankuday@aydin.edu.tr

‡ hasansaygin@aydin.edu.tr

§ senol˙a@ibu.edu.tr

¶ orhancakir@aydin.edu.tr; ocakir@science.ankara.edu.tr

I. INTRODUCTION

The Higgs sector of the Standard Model (SM) is in the minimal form, which contains one complex isospin doublet of scalar fields (ϕ^+, ϕ^0), resulting in one physical neutral CP-even Higgs boson (h^0) which has been discovered at the LHC by ATLAS [1] and CMS [2] collaborations. However, there are many possibilities for the extension of the Higgs sector, introducing further multiplets of scalar fields, which might be singlets, doublets, or triplets of the symmetry groups. The extended Higgs sectors are more relevant to the neutrino mass, baryogenesis and dark matter. It is thus natural to consider scenarios with additional complex scalars such as two Higgs doublet model (THDM) [3]. The scalar fields (ϕ_1 and ϕ_2) couplings to the up-type, down-type and charged lepton $SU(2)_L$ singlet fermions can be identified for discrete types of the THDM [4, 5]. Model of type-I are the one in which all SM fermions couple to a single scalar field (ϕ_2). In type-II model down-type quarks and charged leptons couple to one scalar field (ϕ_1), while the up-type quarks and neutrinos couple to the other scalar field (ϕ_2). Furthermore, in the model of type-III the quarks couple to one of the scalar field (ϕ_1), while leptons couple to the other (ϕ_2). In the model of type-IV, the couplings of scalar (ϕ_2) to up-type quarks and charged leptons, and the couplings of scalar (ϕ_1) to down-type quarks and neutrinos are present. Here, we consider two types of THDM-I and THDM-II for type-I and type-II of two Higgs doublet model, respectively.

The two Higgs doublets carry opposite hypercharges, the (ϕ_1 and ϕ_2) scalar potential will contain the mixing parameters related to the mass. In this case, the Higgs doublets will have different vacuum expectations values (v_1 and v_2). The massive SM gauge bosons acquire their masses from the expressions with the vacuum expectation value $v = (v_1^2 + v_2^2)^{1/2}$. After the spontaneous symmetry breaking there appears five physical scalar particles: two neutral CP-even bosons h^0 and H^0, one neutral CP-odd boson A^0, and two charged bosons $H^\pm$. Phenomenologically, the two Higgs doublet model includes the free parameters: mixing angle, the ratio of the vacuum expectation values ($\tan\beta = v_2/v_1$), the masses of Higgs bosons. In the extended models of multiple neutral scalar bosons, the mixing between them would make it difficult to identify their properties. Therefore, it is important to study the charged scalar bosons, which could provide unique signatures to distinguish the models with extended Higgs sector.

Constraints on the charged Higgs bosons in the THDM are given from both low energy

flavour experiments and high energy collider experiments. The direct lower bounds on the charged Higgs boson mass $m_{H^\pm}$ come from LEP experiments. They were sensitive to the masses of charged Higgs boson up to about 90 GeV, in two decay channels of $H^+ \to \tau^+\nu$ and $H^+ \to c\bar{s}$, and the exclusion limit on the mass independent of the admixture of these branching fractions was 78.9 GeV [4]. Assuming the THDM-II model the lower bounds are 87.8 GeV for large $\tan\beta$ values using the decay mode $H^+ \to \tau^+\nu$ and 80.4 GeV for relatively low $\tan\beta$ values. Using the bounds $m_{A^0} > 92$ GeV and the characteristic relation $m_{H^\pm} = (m^2_{A^0} + m_{W^\pm})^{1/2}$ (as in the MSSM), one obtains the bound $m_{H^\pm} > 122$ GeV. In the model THDM-II the mass of charged Higgs boson is constrained by the precision measurements of the radiative decay of $B \to X_s\gamma$ by the low energy experiments. The lower bound on the mass $m_{H^\pm} > 295$ GeV are given for the model THDM-II. The decay $B \to \tau\nu$ can also be used to constrain the charged Higgs parameters, being sensitive to $(\tan\beta/m_{H^\pm})^2$, which yields a lower bound $m_{H^\pm} > 300$ GeV for $\tan\beta > 40$. A study of data analysis based on $b \to s\gamma$ [6] have excluded a mass range up to 380 GeV in a variety of interesting processes and BSM scenarios. However, these bounds can be relaxed if the MSSM or other new physics models contributes through the loop diagrams.

Beyond the search channels for a Standard Model Higgs boson, the LHC experiments are exploring additional channels that are specific to extended Higgs bosons. ATLAS [7] and CMS [8] collaborations have already performed a number of extended Higgs searches which exclude $\tan\beta > 50$ in the range of heavy charged Higgs, $m_{H^\pm} > 200$ GeV. Recently, the CMS collaboration [9] have put 95% C.L. exclusion limit on the mass of the charged Higgs boson in 180-600 GeV mass range. This search is performed at a center of mass energy of 8 TeV with 19.7 fb^{-1} of data from $pp \to \bar{t}(b)H^+$ and $pp \to t(\bar{b})H^-$ production processes with $H^+ \to \tau^+\nu_\tau$ decay mode. The ATLAS collaboration [10] have searched for charged Higgs bosons decaying through $H^\pm \to \tau^\pm\nu_\tau$ process using the proton-proton collision data at $\sqrt{s} = 8$ TeV with 19.5 fb^{-1}, the results exclude a large range of $\tan\beta$ values for charged Higgs boson masses in the range $80-160$ GeV, and exclude parameter space with high $\tan\beta$ for the range of mass $m_{H^\pm} = 200 - 250$ GeV.

The searches of the heavy Higgs bosons of the THDM have special challenge at present high energy colliders. One of the future international projects currently under consideration is the Future Circular Collider (FCC) [11] which has the potential to search for a wide parameter range of new physics. The FCC-hh collider is to provide proton-proton collisions

at nearly an order of magnitude higher energy than the LHC, the proposed centre-of-mass energy is 100 TeV and the peak luminosity is 5×10^{34} cm^{-2}s^{-1} [12].

In this work, we study the processes $pp \to t\bar{t}b(\bar{b}) + X$ for the signal and background at the FCC-hh collider. Our analysis is focused on the production of a pair of top quarks and associated bottom quark for the charged Higgs boson search within the THDM-I and THDM-II in the pp collisions at very high energy frontier. We have obtained the significant coverage of the parameter space at large integrated luminosity projections for the FCC-hh collider. We define the relevant expressions for the $H^- q\bar{q}$ and $H^- l^+ \bar{\nu}$ couplings as well as scalar-vector-scalar ($H^- W^+ h^0$, $H^- W^+ H^0$, $H^- W^+ A^0$) couplings in section II. We present the calculation for the decay widths and branchings ratios of the charged Higgs boson in section III. In section IV, we plot the production cross section according to the mass of charged Higgs boson for two types of THDM at the center of mass energy $\sqrt{s} = 100$ TeV of the pp collisions. Finally, the results from the analysis of the signal and background are given in section V.

II. CHARGED HIGGS BOSON COUPLINGS

The magnitude of the couplings for $H^- f_i \bar{f}_j$ interactions are given by

$$g_{H^- q_i \bar{q}_j} \equiv g|V_{q_i q_j}|[m_{q_i} \cot\beta(1+\gamma_5) + T_x m_{q_j} \tan\beta(1-\gamma_5)]/(2\sqrt{2}m_W) \tag{1}$$

$$g_{H^- \nu_i l_j^+} \equiv g|U_{\nu_i l_j}|[T_x m_{l_j} \tan\beta(1-\gamma_5)]/(2\sqrt{2}m_W) \tag{2}$$

where $V_{q_i q_j}$ and $U_{\nu_i l_j}$ are the CKM matrix elements in quark sector and PMNS matrix elements in lepton sector, respectively. The g is the weak coupling constant, the $\tan\beta$ is the ratio of vacuum expectation vales of the Higgs doublets. The m_q and m_l are the corresponding quark and lepton masses, respectively. We use the parameter T_x to identify the type of THDM such that $T_I = -\cot\beta/\tan\beta$ denotes THDM-I and $T_{II} = 1$ denotes THDM-II.

The couplings for $H^- W^+ h^0$, $H^- W^+ H^0$ and $H^- W^+ A^0$ interactions can be written by

$$g_{H^- W^+ h^0} \equiv g\cos(\beta-\alpha)(p_{H^-} + p_{h^0})/2 \tag{3}$$

$$g_{H^-W^+H^0} \equiv g\sin(\beta-\alpha)(p_{H^-}+p_{H^0})/2 \tag{4}$$

$$g_{H^-W^+A^0} \equiv ig(p_{H^-}+p_{A^0})/2 \tag{5}$$

where the p_{h^0}, p_{H^0}, p_{A^0} and p_{H^-} are the four-momenta for neutral Higgs bosons and charged Higgs boson, respectively. We use the expression for the angle factor of $\cos^2(\beta-\alpha) = [(m^2_{h^0}/m^2_Z)(m^2_{h^0}/m^2_Z-1)]/[(m^2_{H^0}/m^2_Z-m^2_{h^0}/m^2_Z)(m^2_{H^0}/m^2_Z+m^2_{h^0}/m^2_Z-1)]$. By implementing the relevant interaction vertices into the CalcHEP [13] package, we calculate the decay width and branching ratios as well as the process cross section for different parametrizations (PI for $m_{A^0} = 100$ GeV and $m_{H^0} = m_{H^-}$, PII for $m_{A^0} = m_{H^0} = m_{H^-}$) within the THDM-I and THDM-II.

III. DECAY WIDTH AND BRANCHING RATIOS

The partial decay widths of charged Higgs boson into fermionic channels can be calculated as

$$\begin{aligned}\Gamma(H^- \to q_i\bar{q}_j) = &\frac{3g^2\lambda^{1/2}(m^2_{H^-}, m^2_{q_i}, m^2_{q_j})}{32\pi m^2_W m^3_{H^-}}|V_{q_iq_j}|^2 \\ &\times\left[(m^2_{H^-}-m^2_{q_j}-m^2_{q_i})(T^2_x m^2_{q_j}\tan^2\beta + m^2_{q_i}\cot^2\beta) - 4T_x m^2_{q_j}m^2_{q_i}\right]\end{aligned} \tag{6}$$

$$\Gamma(H^- \to \bar{\nu}_i l^-_j) = \frac{g^2\lambda^{1/2}(m^2_{H^-}, m^2_{l_j}, 0)}{32\pi m^2_W m^3_{H^-}}|U_{\nu_i l_j}|^2\left[T^2_x(m^2_{H^-}-m^2_{l_j})m^2_{l_j}\tan^2\beta\right] \tag{7}$$

where $\lambda^{1/2}$ is a kinematic factor of mass squared dimension and it can be defined as $\lambda(m^2_1, m^2_2, m^2_3) = [(m^2_1+m^2_2-m^2_3)^2 - 4m^2_1m^2_2]$. For the channels $H^- \to W^-h^0$, $H^- \to W^-H^0$ and $H^- \to W^-A^0$ we calculate the decay widths

$$\begin{aligned}\Gamma(H^- \to W^-h^0) = &\frac{g^2\lambda^{1/2}(m^2_{H^-}, m^2_W, m^2_{h^0})\cos^2(\beta-\alpha)}{64\pi m^3_{H^-}} \\ &\times\left[m^2_W - 2(m^2_{H^-}+m^2_{h^0}) + \frac{(m^2_{H^-}-m^2_{h^0})^2}{m^2_W}\right]\end{aligned} \tag{8}$$

$$\Gamma(H^- \to W^-H^0) = \frac{g^2\lambda^{1/2}(m^2_{H^-}, m^2_W, m^2_{H^0})\sin^2(\beta-\alpha)}{64\pi m^3_{H^-}}$$

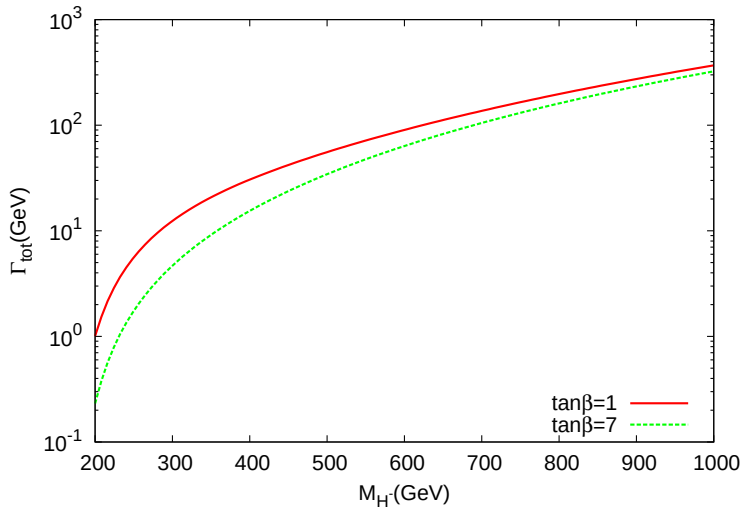


Figure 1. Decay width of $H^{\pm}$ boson depending on its mass for different values of $\tan\beta$ and parameter set PI of THDM-I.

$$\times \left[m_W^2 - 2(m_{H^-}^2 + m_{H^0}^2) + \frac{(m_{H^-}^2 - m_{H^0}^2)^2}{m_W^2} \right] \tag{9}$$

$$\Gamma(H^- \to W^- A^0) = \frac{g^2 \lambda^{1/2}(m_{H^-}^2, m_W^2, m_{A^0}^2)}{64\pi m_{H^-}^3} \times \left[m_W^2 - 2(m_{H^-}^2 + m_{A^0}^2) + \frac{(m_{H^-}^2 - m_{A^0}^2)^2}{m_W^2} \right] \tag{10}$$

The decay widths of the charged Higgs boson for the models THDM-I and THDM-II are presented in Fig. 1-4. It is shown that the decay width for model THDM-I is larger than that for THDM-II in the considered parameter space. The decay width increases with the charged Higgs boson mass for parameter PI of THDM-I, while it slightly changes depending on the mass $m_{H^-} > 300$ GeV for parameter PII of THDM-I, and it is almost constant for large $\tan\beta$. In the model THDM-II, the decay width shows a minimum around $\tan\beta \approx 7$. As an example, using the parametrization PI (PII) of THDM-II, the mass $m_{H^-} = 300$ GeV and $\tan\beta = 7$, the decay width is obtained $\Gamma = 5.0 \times 10^0$ (3.5×10^{-1}) GeV as in Fig. 3 (4), respectively.

For the parameter set PI and PII of THDM-I, the branching ratios of charged Higgs boson into different decay channels are given in Fig. 5-6. For a mass value of $m_{A^0} > 100$ GeV the branching into the channel $H^- \to \bar{t}b$ becomes dominant as shown in Fig. 6. The branching ratios are given in Fig. 7-10 for the parameter set PI and PII of THDM-II.

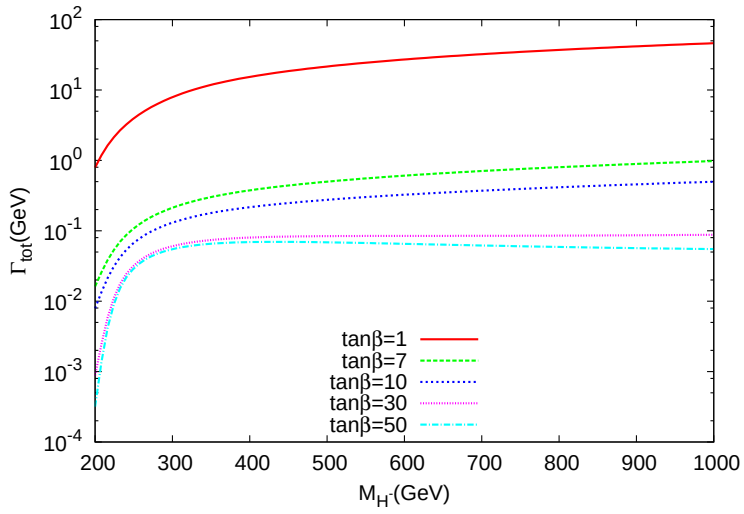


Figure 2. Decay width of $H^{\pm}$ boson depending on its mass for parameter set PII of model THDM-I.

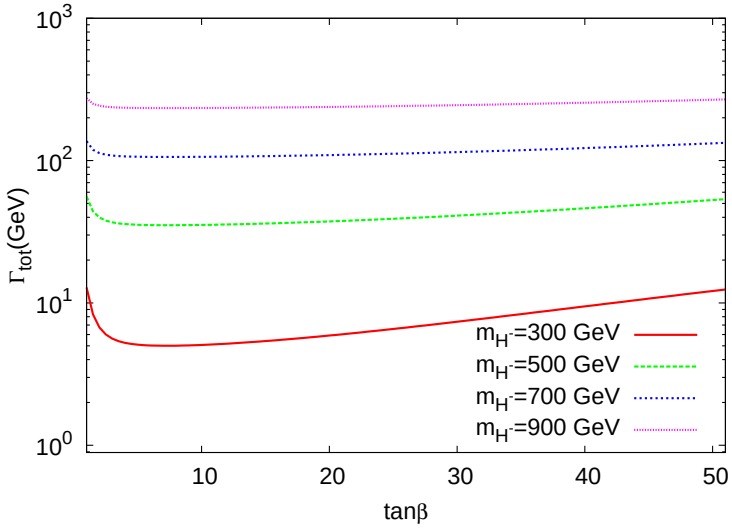


Figure 3. Decay width of $H^{\pm}$ boson depending on $\tan\beta$ for different mass of charged Higgs boson for parameter set PI of model THDM-II.

IV. PRODUCTION CROSS SECTION AT FCC-HH COLLIDER

The ongoing searches at the LHC rely on specific production and decay mechanism that occupy only a part of the complete model parameter space. The cross sections for the single production of charged Higgs boson through the process $pp \to tH^- + X$ within the THDM-I and THDM-II are presented in Fig. 11 and 12. The characteristics of the cross

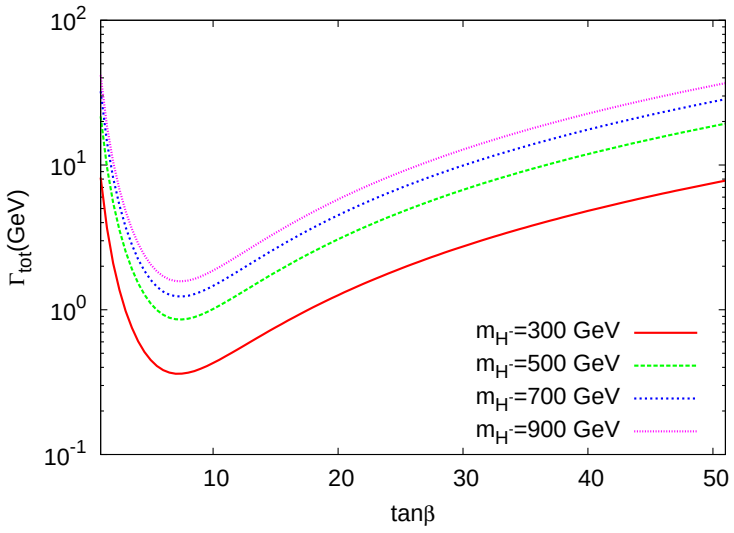


Figure 4. Decay width of $H^{\pm}$ boson depending on $\tan\beta$ for different mass values of charged Higgs boson for parameter set PII of model THDM-II.

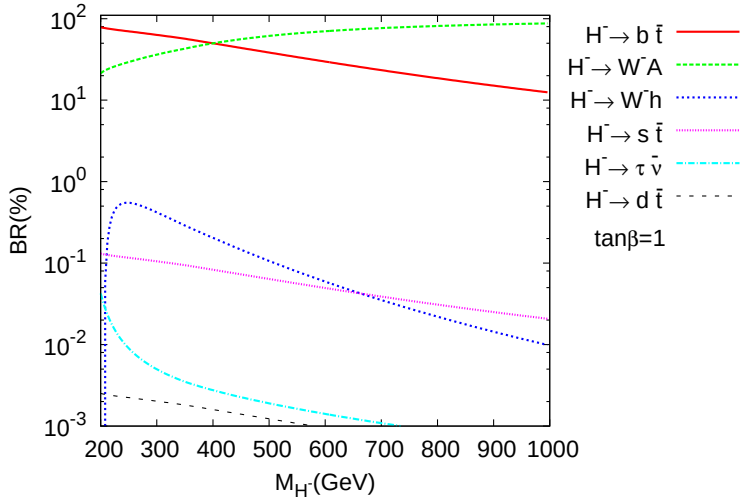


Figure 5. Branching ratios to different decay modes of charged Higgs boson depending on $\tan\beta$ and parameter set PI of model THDM-I.

sections depending on the $\tan\beta$ can be seen from these figures as expected from the $H^- f_i \bar{f}_j$ interaction vertices. The cross sections have a minimum around $\tan\beta \approx 7$ for THDM-II while it decreases with the increasing values of $\tan\beta$ for THDM-I. There exist large values of cross section $\sigma \simeq 37.5$ pb for $\tan\beta = 1$, however it is 0.8 pb (1.5 pb) for $\tan\beta = 7$ within the model THDM-I (THDM-II), respectively. For large values of $\tan\beta$ the cross

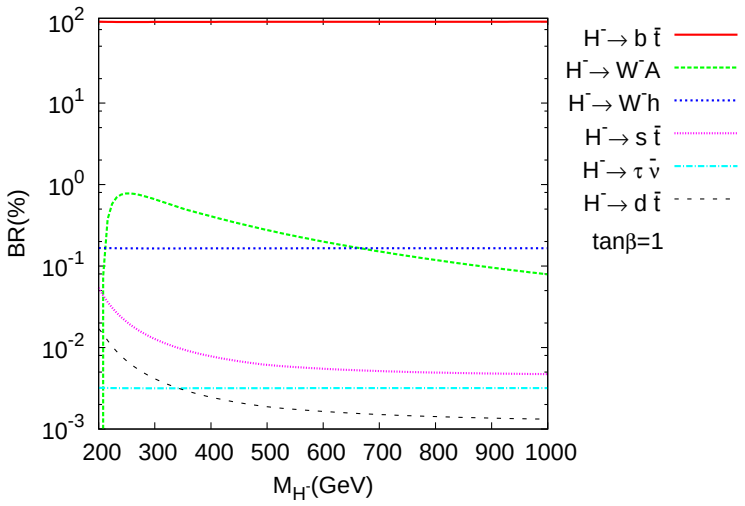


Figure 6. Branching ratios to different decay modes of charged Higgs boson depending on $\tan\beta$ and parameter set PII of model THDM-I.

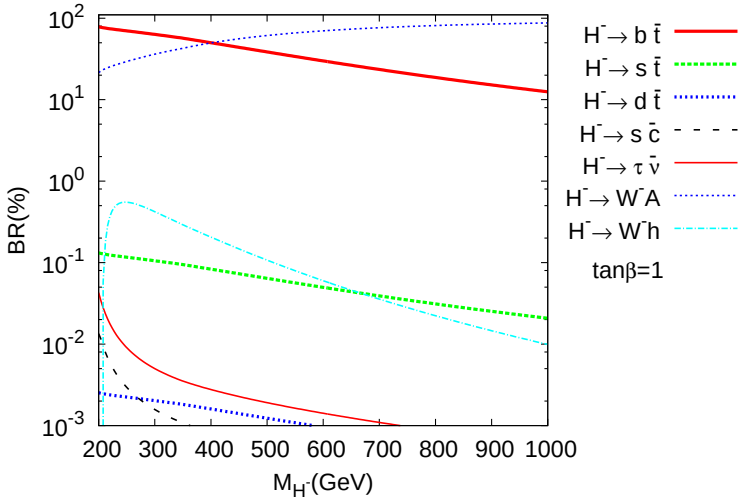


Figure 7. Branching ratios to different decay modes of charged Higgs boson depending on its mass for $\tan\beta = 1$ and parameter set PI of model THDM-II.

section decreases for THDM-I, while it is in the same level (comparing the cross sections at $\tan\beta = 1$ and $\tan\beta \simeq 50$) for THDM-II.

In order to examine the kinematical distributions of associated $b(\bar{b})$ quark, the transverse momentum distributions of $b(\bar{b})$ quarks for the process $pp \to t\bar{t}b(\bar{b}) + X$ are presented in Fig. 13 and 14 for the parameter set PI and PII of THDM-I, respectively. Fig. 15 and 16 show

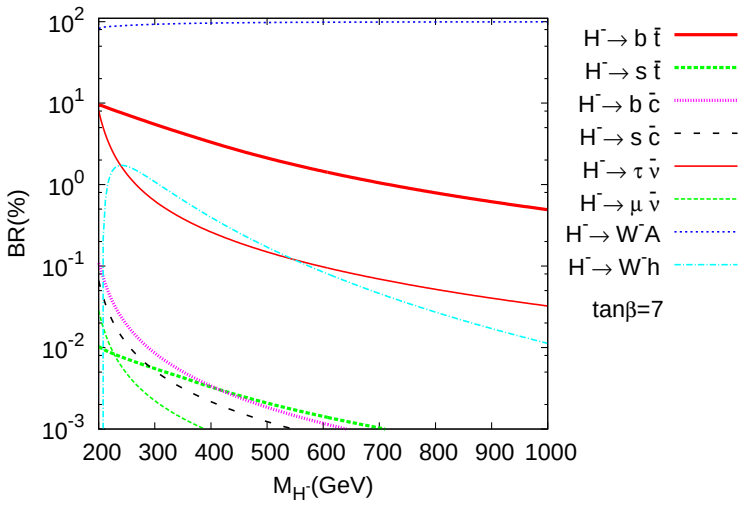


Figure 8. Branching ratios to different decay modes of charged Higgs boson depending on its mass for $\tan\beta = 7$ and parameter set PI of model THDM-II.

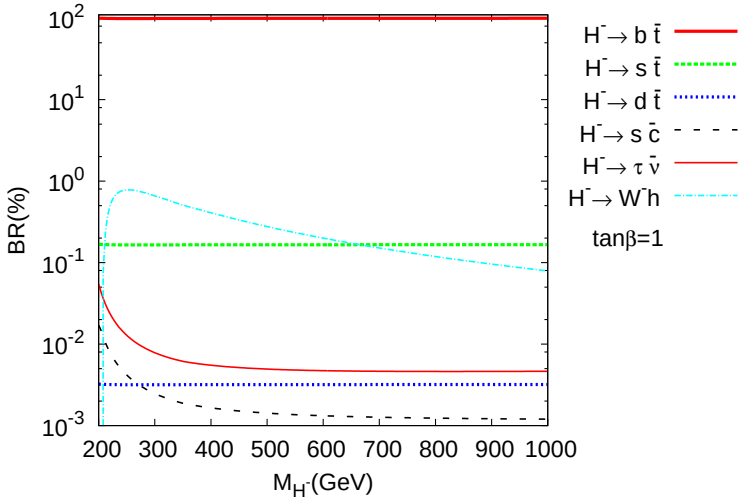


Figure 9. Branching ratios to different decay modes of charged Higgs boson depending on its mass for $\tan\beta = 1$ for parameter set PII and model THDM-II.

the pseudorapidity distributions of $b(\bar{b})$ quarks for parameter set PI and PII of THDM-I, respectively. The invariant mass distributions m_{tb} (t and $b(\bar{b})$ quark in the final state) are presented in Fig. 17 and 18 for parameter PI and PII of THDM-I, respectively.

Transverse momentum distributions of $b(\bar{b})$ quarks are presented in Fig. 19 and 20 for parameter set PI and PII of THDM-II, respectively. Fig. 21 and 22 show the pseudorapidity

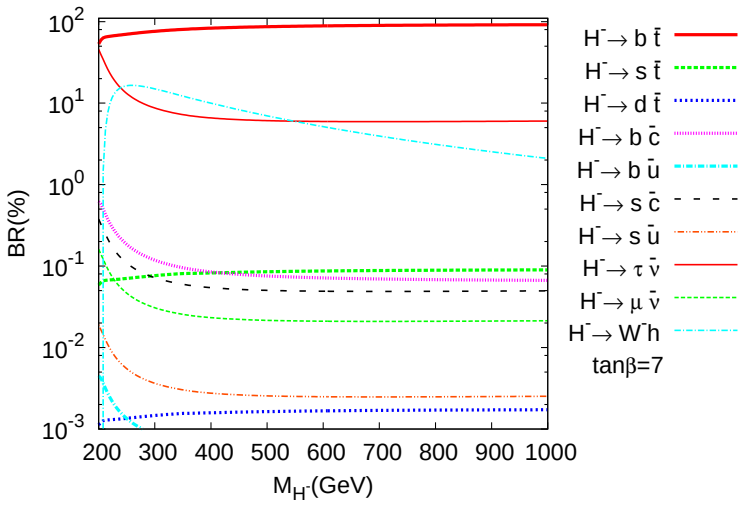


Figure 10. Branching ratios to different decay modes of charged Higgs boson depending on its mass for $\tan\beta = 7$ for parameter set PII and model THDM-II.

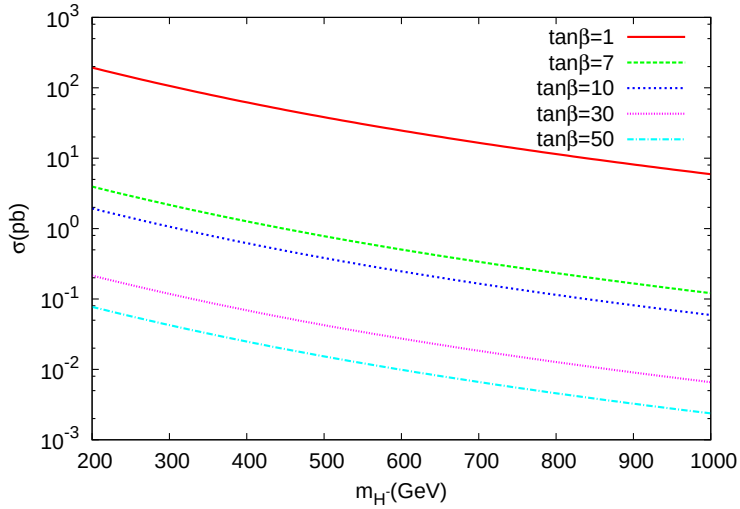


Figure 11. Cross section for charged Higgs boson production within the THDM-I at FCC-hh collider.

distributions of $b(\bar{b})$ quarks for parameter set PI and PII of THDM-II, respectively. The invariant mass distributions m_{tb} (top and bottom quark in the final state) are presented in Fig. 23 and 24 for parameter PI and PII of THDM-II, respectively.

The cross sections for the background processes $pp \to t\bar{t}b(\bar{b}) + X$, $pp \to t\bar{t}c(\bar{c}) + X$ and $pp \to t\bar{t}j + X$ are presented in Table I for the center of mass energy $\sqrt{s} = 100$ TeV of

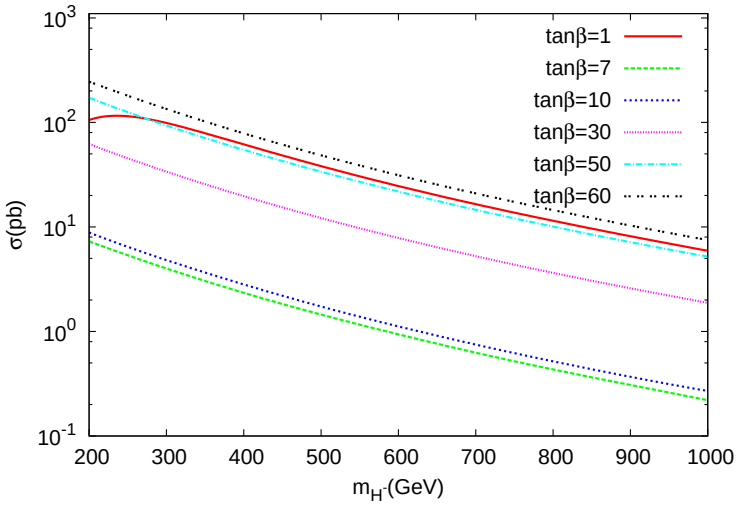


Figure 12. Cross section for charged Higgs boson production within the THDM-II at FCC-hh collider.

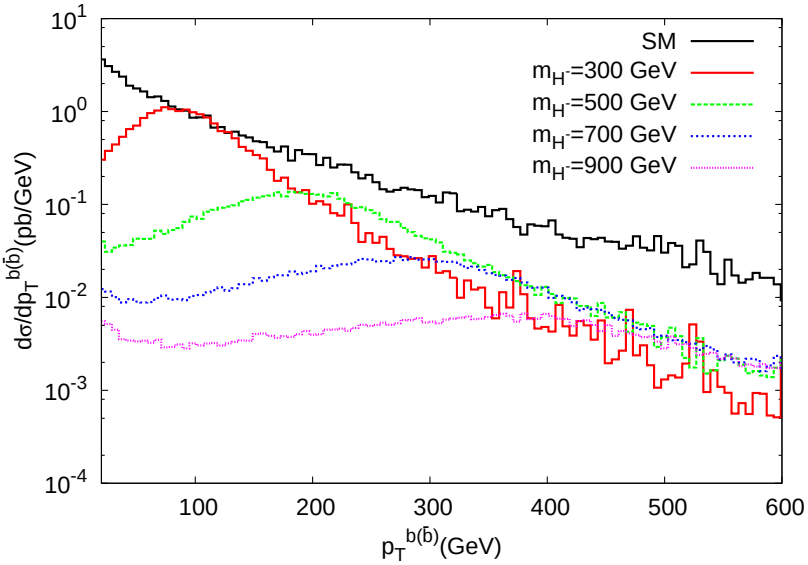


Figure 13. Transverse momentum distributions of $b(\bar{b})$ quarks for set PI of THDM-I.

FCC-hh collider. In the study we consider the background due to one leading b-jet. Other b-jets originating from top quark decays will have different kinematical distributions from the top-antitop associated leading one. In addition to the basic kinematical cuts $p_T > 20$ GeV and $|\eta| < 2.5$ an invariant mass cut $|m_{tb} - m_{H^\pm}| \leq 0.1 m_{H^\pm}$ is applied for the analysis. For the calculation of background cross section $\Delta\sigma_B$ within the invariant mass interval

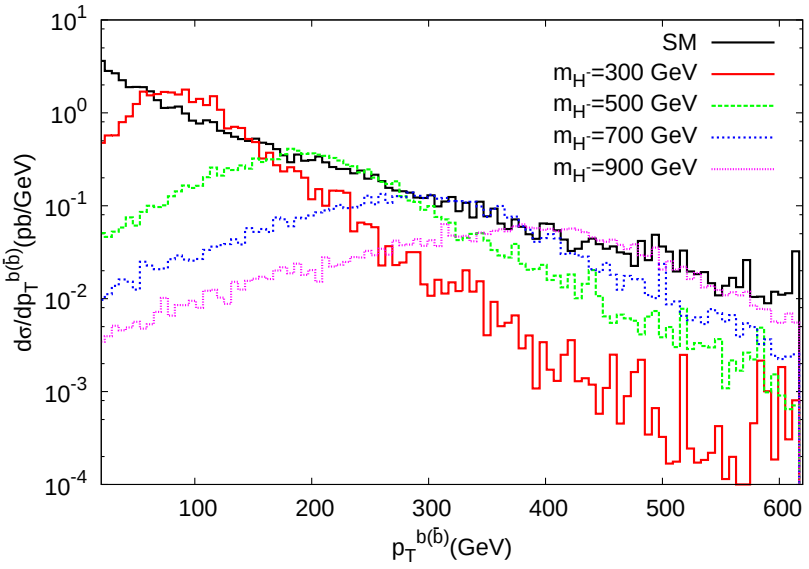


Figure 14. Transverse momentum distributions of $b(\bar{b})$ quarks for parameter PII of THDM-I.

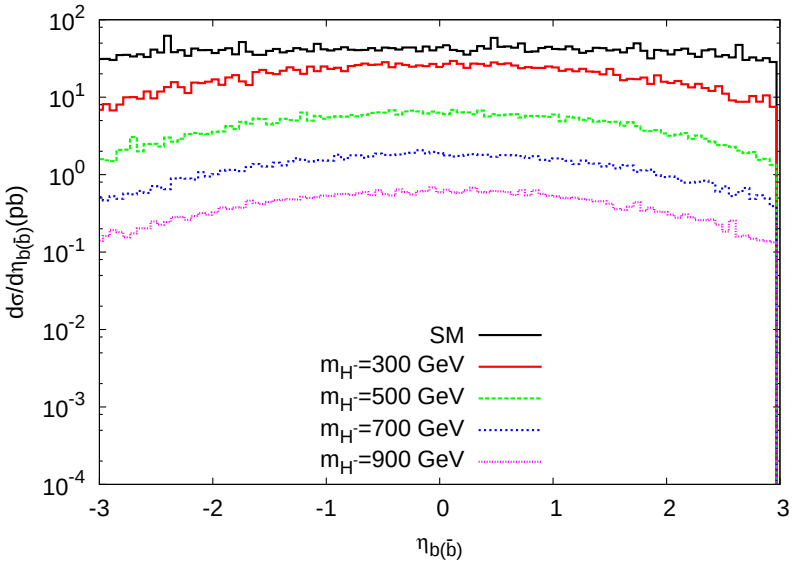


Figure 15. Pseudorapidity distributions of $b(\bar{b})$ quarks for set PI of THDM-I.

$|m_{tb} - m_{H^\pm}| \leq 0.1 m_{H^\pm}$, we assume the efficiency of b-tagging to be $\epsilon_b = 50\%$ and the rejection ratios to be 10% for $c(\bar{c})$ quark jets and 1% for light quark jets since they are assumed to be mistagged as b-jets.

In Tables II-V we present the signal cross sections $\Delta\sigma_S$ within the invariant mass interval $|m_{tb} - m_{H^\pm}| \leq 0.1 m_{H^\pm}$, for single production of charged Higgs boson in the model framework

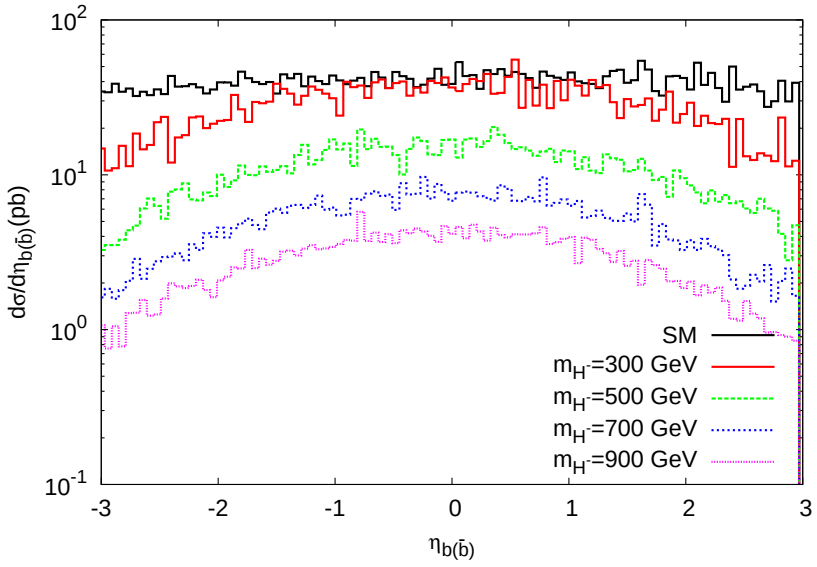


Figure 16. Pseudorapidity distributions of $b(\bar{b})$ quarks for parameter PII of THDM-I.

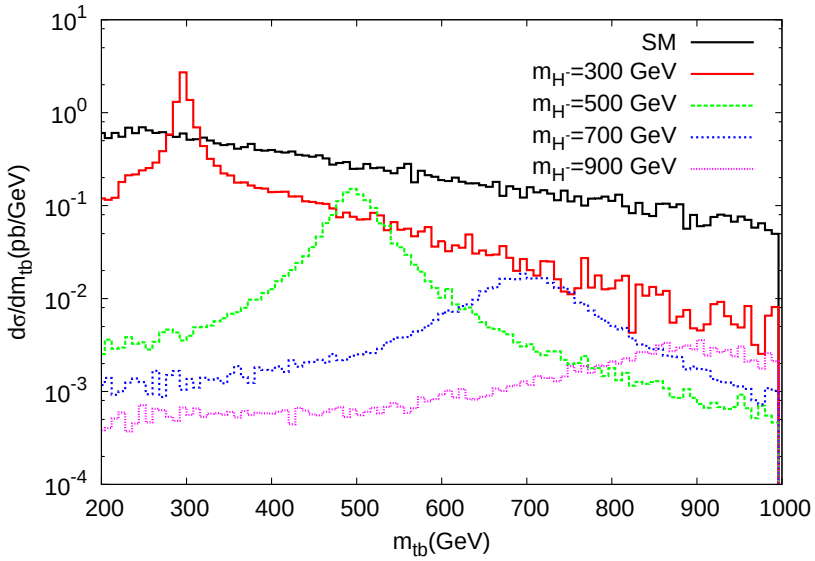


Figure 17. Invariant mass distributions of $b(\bar{b})$ quarks for set PI of THDM-I.

of THDM-I and THDM-II (for the parametrizations PI and PII) at FCC-hh collider with $\sqrt{s} = 100$ TeV.

The final states result from the decays of W bosons for $W^+W^- + 3b_{jet}$ (where we assume at least one W boson decays leptonically or both W bosons decay leptonically). In Table VI, the statistical significances $S/\sqrt{B}$ (where S is the number of signal events and B is

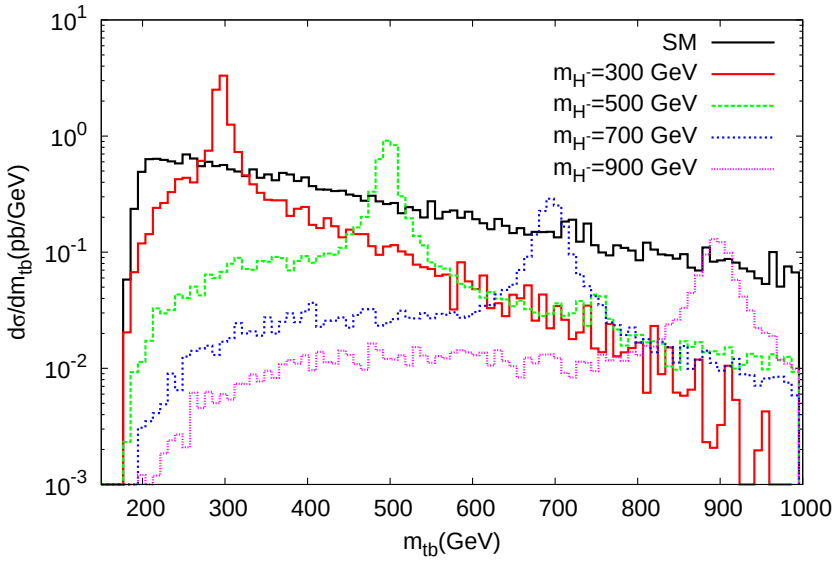


Figure 18. Invariant mass distributions of $b(\bar{b})$ quarks for parameter PII of THDM-I.

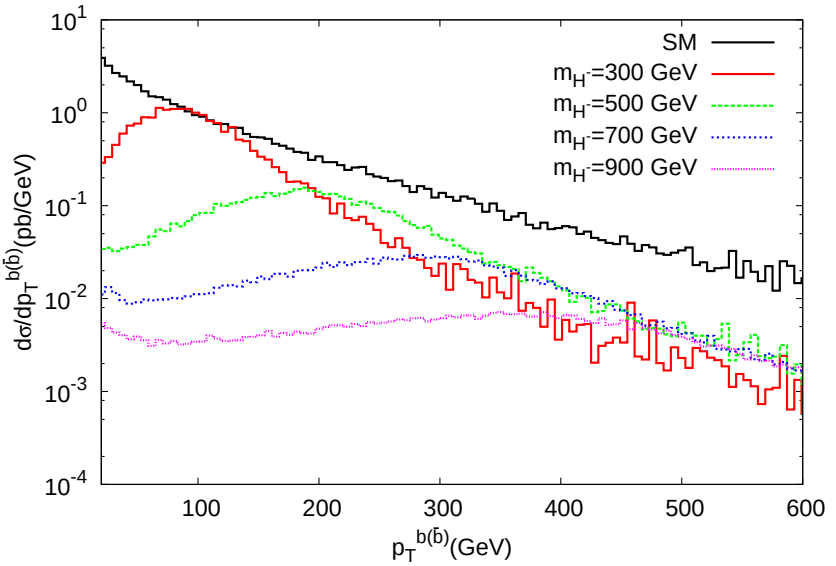


Figure 19. Transverse momentum distributions of $b(\bar{b})$ quarks for set PI of THDM-II.

the number of background events) for the integrated luminosity of $L_{int} = 500$ fb^{-1}, and different types (THDM-I and THDM-II) and parametrizations (PI and PII) of the model are presented.

In Figures 25 - 26, we present the luminosity requirement for the signal observability depending on the mass of charged Higgs boson in the channel - one W boson decays hadron-

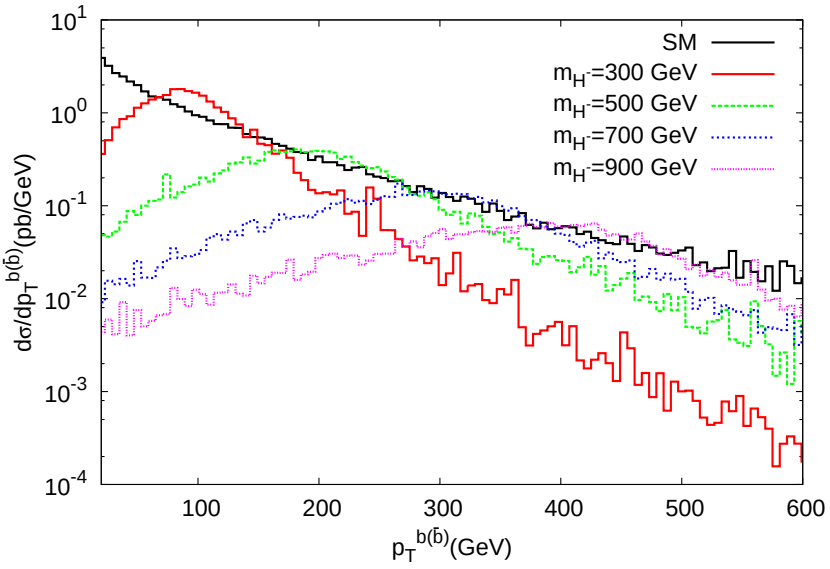


Figure 20. Transverse momentum distributions of $b(\bar{b})$ quarks for parameter PII of THDM-II.

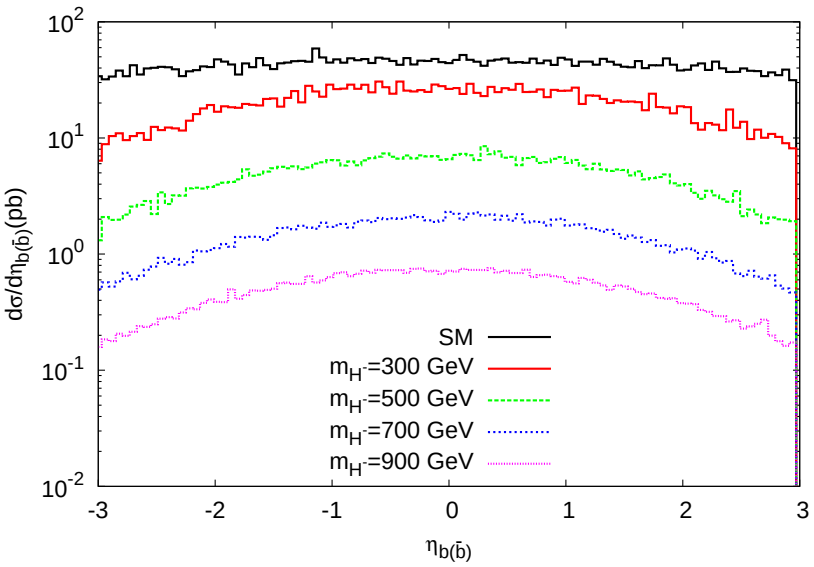


Figure 21. Pseudorapidity distributions of $b(\bar{b})$ quarks for set PI of THDM-II.

ically while the other decays leptonically (channel - both W bosons decay leptonically) for single production of charged Higgs boson within the model framework of THDM-II (parametrization PII) at FCC-hh with $\sqrt{s} = 100$ TeV. The results are shown in different types of lines for different $\tan\beta$ values.

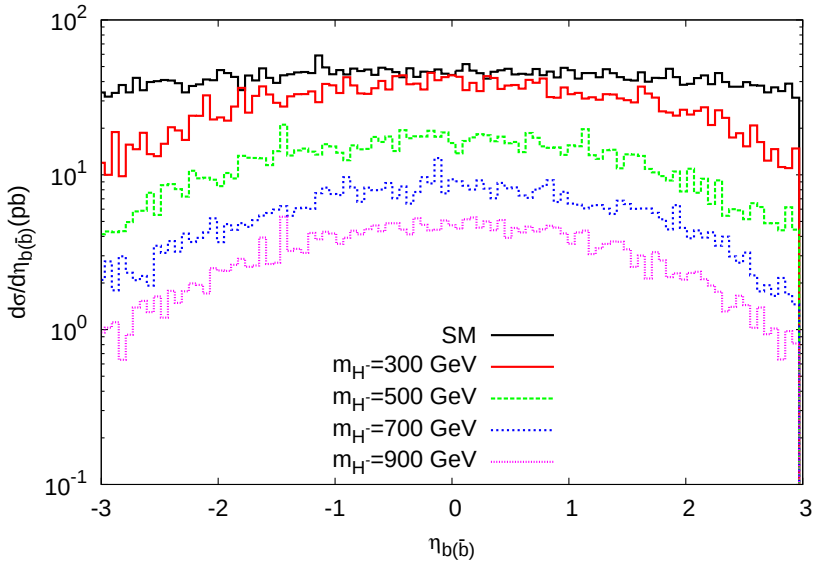


Figure 22. Pseudorapidity distributions of $b(\bar{b})$ quarks for parameter PII of THDM-II.

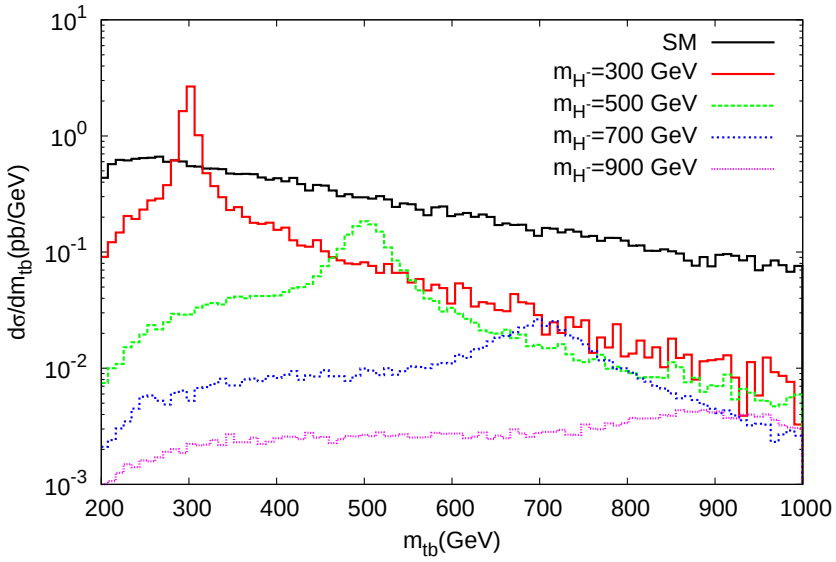


Figure 23. Invariant mass distributions of $b(\bar{b})$ quarks for set PI of THDM-II.

V. CONCLUSIONS

Possible extensions of the Higgs sector can be searched for a wide range of parameter space in the high energy proton-proton collisions. The ongoing searches at the LHC rely on specific production and decay mechanism that occupy only a part of the complete model parameter space. The decay modes of the Higgs bosons can be well similar to the background

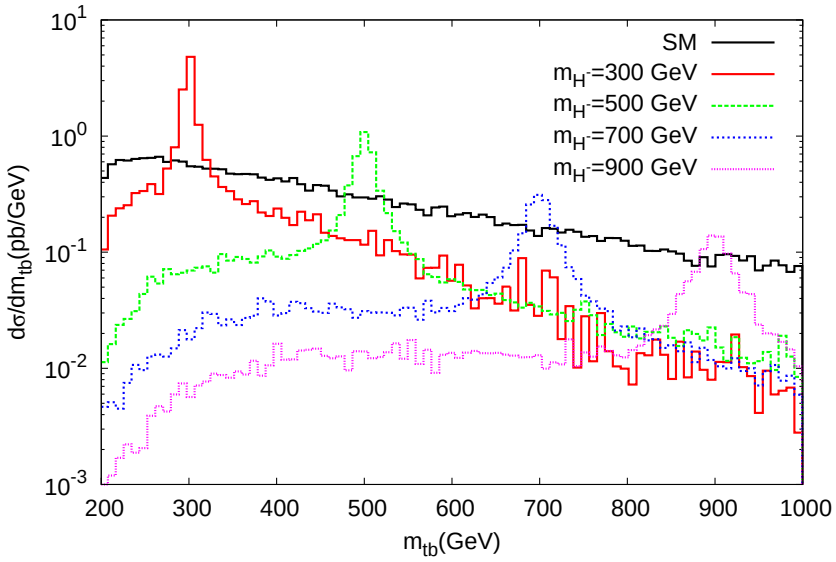


Figure 24. Invariant mass distributions of $b(\bar{b})$ quarks for parameter PII of THDM-II.

Table I. The cross sections (in pb) for the background processes $pp \to t\bar{t}b(\bar{b}) + X$, $pp \to t\bar{t}c(\bar{c}) + X$ and $pp \to t\bar{t}j + X$ calculated in the invariant mass range $|m_{tb} - m_{H^\pm}| \leq 0.1 m_{H^\pm}$ at the center of mass energy $\sqrt{s} = 100$ TeV.

m_{tb} (GeV)	$pp \to t\bar{t}b(\bar{b}) + X$	$pp \to t\bar{t}c(\bar{c}) + X$	$pp \to t\bar{t}j + X$	$\Delta\sigma_B(pb)$
300 ± 30	2.99×10^0	3.65×10^0	2.51×10^2	4.37×10^0
500 ± 50	2.88×10^0	3.62×10^0	1.23×10^2	3.03×10^0
700 ± 70	1.89×10^0	2.40×10^0	8.04×10^1	1.99×10^0
900 ± 90	1.34×10^0	1.86×10^0	5.47×10^1	1.40×10^0

Table II. The cross sections for the signal process $pp \to t\bar{t}b(\bar{b}) + X$ within the THDM-I and parametrization PI calculated in the invariant mass range $|m_{tb} - m_{H^\pm}| \leq 0.1 m_{H^\pm}$ at the center of mass energy $\sqrt{s} = 100$ TeV.

THDM-I and PI	$\Delta\sigma_S(pb)$			
m_{tb} (GeV)	$\tan\beta = 1$	$\tan\beta = 7$	$\tan\beta = 30$	$\tan\beta = 50$
300 ± 30	1.24×10^1	1.30×10^{-2}	4.09×10^{-5}	5.02×10^{-6}
500 ± 50	2.29×10^0	1.97×10^{-3}	5.02×10^{-6}	5.96×10^{-7}
700 ± 70	5.52×10^{-1}	4.60×10^{-4}	8.99×10^{-7}	1.19×10^{-7}
900 ± 90	1.13×10^{-1}	6.59×10^{-5}	2.43×10^{-7}	2.54×10^{-8}

Table III. The same as II, but for the THDM-I and PII.

THDM-I and PII	$\Delta\sigma_S(pb)$			
m_{tb} (GeV)	$\tan\beta = 1$	$\tan\beta = 7$	$\tan\beta = 30$	$\tan\beta = 50$
300 ± 30	1.88×10^{1}	7.16×10^{-2}	4.21×10^{-4}	7.57×10^{-5}
500 ± 50	8.33×10^{0}	5.56×10^{-2}	1.94×10^{-4}	5.03×10^{-5}
700 ± 70	3.41×10^{0}	1.84×10^{-2}	1.64×10^{-4}	3.02×10^{-5}
900 ± 90	1.59×10^{0}	1.72×10^{-2}	9.28×10^{-5}	6.32×10^{-6}

Table IV. The same as II, but for the THDM-II and PI.

THDM-II and PI	$\Delta\sigma_S(pb)$			
m_{tb} (GeV)	$\tan\beta = 1$	$\tan\beta = 7$	$\tan\beta = 30$	$\tan\beta = 50$
300 ± 30	1.22×10^{1}	3.57×10^{-2}	5.22×10^{-1}	7.24×10^{0}
500 ± 50	2.45×10^{0}	5.26×10^{-3}	3.48×10^{-1}	2.02×10^{0}
700 ± 70	3.90×10^{-1}	9.37×10^{-4}	6.08×10^{-2}	2.97×10^{-1}
900 ± 90	1.00×10^{-1}	1.86×10^{-4}	1.24×10^{-2}	8.59×10^{-2}

reactions from top and bottom quarks and other sources. If the single production of charged Higgs boson associated with top quark is observed at the LHC, one of the following questions is to identify the $H^- t\bar{b}$ interaction. The studies on the observables related to the angular distribution of charged lepton in the final state and the forward-backward asymmetry can be found in [14] and references therein. Even it seems challenging to measure precisely due to the large hadronic background and systematic uncertainties, we look forward to its

Table V. The same as II, but for the THDM-II and PII.

THDM-II and PII	$\Delta\sigma_S(pb)$			
m_{tb} (GeV)	$\tan\beta = 1$	$\tan\beta = 7$	$\tan\beta = 30$	$\tan\beta = 50$
300 ± 30	1.70×10^{1}	2.12×10^{-1}	3.70×10^{0}	1.12×10^{1}
500 ± 50	8.68×10^{0}	6.14×10^{-2}	1.50×10^{0}	4.96×10^{0}
700 ± 70	2.59×10^{0}	2.72×10^{-2}	7.25×10^{-1}	1.97×10^{0}
900 ± 90	1.21×10^{0}	1.24×10^{-2}	5.13×10^{-1}	1.18×10^{0}

Table VI. The statistical significances $S/\sqrt{B}$ at integrated luminosity $L_{int} = 500$ fb^{-1} for different types (THDM-I and THDM-II) and parametrizations (PI and PII) of the model. The numbers in the parenthesis show the results for the channel both W-boson decay leptonically.

Model ($\tan\beta = 1$)	THDM-I		THDM-II	
m_{tb} (GeV)	PI	PII	PI	PII
300 ± 30	402.65 (230.73)	612.95 (351.24)	395.02 (226.35)	553.09 (316.93)
500 ± 50	89.53 (51.30)	324.52 (185.96)	95.45 (54.69)	338.11 (193.75)
700 ± 70	26.56 (15.22)	164.31 (94.16)	18.76 (10.75)	124.56 (71.38)
900 ± 90	6.50 (3.73)	91.53 (52.45)	5.73 (3.61)	69.53 (39.84)

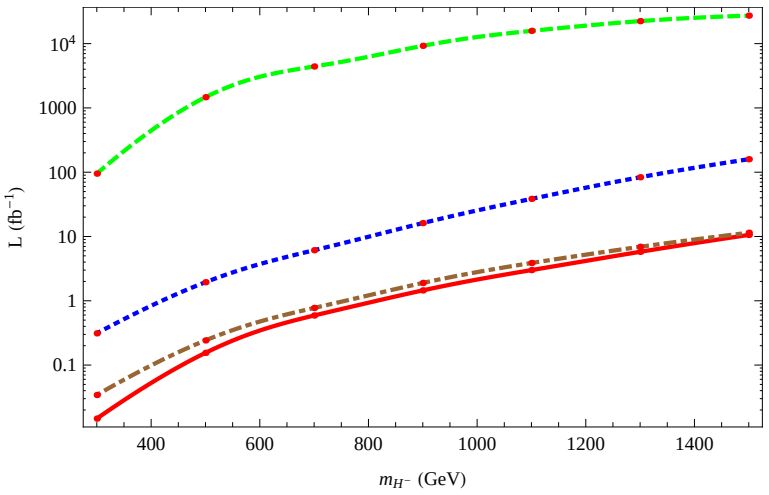


Figure 25. The luminosity need to obtain a 3σ significance depending on the mass of charged Higgs boson and different $\tan\beta$ values (solid line for $\tan\beta = 1$, dashed line for $\tan\beta = 7$, dotted line for $\tan\beta = 30$, dot-dashed line for $\tan\beta = 50$) within the THDMs. From the decay modes $t\bar{t}b(\bar{b}) \to 3b_{jet} + 2j + l + MET$, the final state is accounted for at least 3 b-jets, 2 light jets, single charged lepton, and missing transverse momentum.

exploitation in precision LHC physics and FCC physics scenarios. It is shown that with an integrated luminosity of 500 fb^{-1} at the center of mass energy $\sqrt{s} = 100$ TeV of FCC-hh collider, the signal can be distinguished from the background for the charged Higgs boson

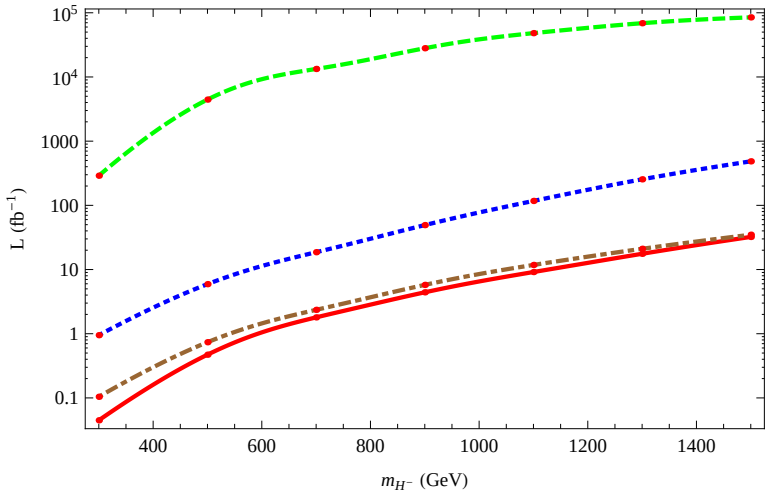


Figure 26. The same as Fig. 25, but for the decay modes $t\bar{t}b(\bar{b}) \to 3b_{jet} + 2l + MET$, the final state is accounted for at least 3 b-jets, 2 opposite charged leptons and missing transverse momentum.

mass up to 1 TeV for a large parameter space of two Higgs doublet model.

---

[1] G. Aad *et al.*, [ATLAS Collaboration], Phys. Lett. B **716**, 1 (2012).

[2] S. Chatrchyan *et al.*, [CMS Collaboration], Phys. Lett. B **716**, 30 (2012).

[3] G.C. Branco *et al.*, Phys. Rept. **516**, 1 (2012).

[4] K.A. Olive *et al.*, Particle Data Group, Chinese Physics C, Vol. **38**, No. 9, 1 (2014).

[5] J.F. Gunion, H.E. Haber, G.L. Kane and S. Dawson, Front. Phys. **80**, 1 (2000).

[6] T. Hermann *et al.*, JHEP **1211**, 036 (2012).

[7] G. Aad *et al.*, [ATLAS Collaboration], ATLAS-CONF-2013-090 (2013).

[8] S. Chatrchyan *et al.*, [CMS Collaboration], CMS PAS HIG-13-026 (2013).

[9] S. Chatrchyan *et al.*, [CMS Collaboration], CMS PAS HIG-14-020 (2014).

[10] G. Aad *et al.*, [ATLAS Collaboration], JHEP **03**, 088 (2015).

[11] The Future Circular Collider Study Group, Kickoff Meeting, 12-15 February 2014, University of Geneva, Switzerland, https://indico.cern.ch/event/282344/. More information is available on the FCC Web site: http://cern.ch/fcc.

[12] A. Ball *et al.*, Future Circular Collider Study Hadron Collider Parameters, FCC-ACC-SPC-0001 (2014).

[13] A. Belyaev, N. Christensen, A. Pukhov, "CalcHEP 3.4 for collider physics within and beyond the Standard Model", Computer Phys. Comm. **184**, 1729 (2013).

[14] X. Gong *et al.*, Modern Phys. Lett. A **29**, No.13, 1430013 (2014).